

Experimental Section

Synthesis of SnS_{2-x}/CC

All the chemicals were used as received without further purification. Typically, a piece of carbon cloth (CC, 2 cm × 4 cm) was ultrasonically treated in concentrated HCl for 2 h, and cleaned with ethanol and distilled water several times. Then, 0.09 mM of SnCl₄·5H₂O and 0.18 mM of thioacetamide were dissolved in 30 mL of deionized water under stirring for 10 min. The mixed solution and pretreated CC were hydrothermally treated in a Teflon-lined stainless-steel autoclave at 180 °C for 24 h. The obtained SnS₂/CC was washed with deionized water and ethanol several times, and dried at 60 °C overnight. Afterwards, SnS₂/CC was treated by Ar plasma for 5 min on an AX-1000 plasma system with a radiofrequency power generator (13.56 MHz) to obtain SnS_{2-x}/CC.

Electrochemical measurements

Electrochemical measurements were carried out on a CHI-660E electrochemical workstation. The graphite rod, Ag/AgCl and CC-loaded catalyst were used as the reference, counter and working electrodes, respectively. All potentials were referenced to reversible hydrogen electrode (RHE) by E (V vs. RHE) = E (V vs. Ag/AgCl) + 0.198 V + 0.059 × pH. The electrocatalytic NORR measurements were performed in NO saturated 0.5 M Na₂SO₄ electrolyte using a gas-tight H-cell. Prior to NORR test, all the feeding gases were purified through two glass bubblers containing 4 M KOH solution and the cathodic compartment was purged with Ar for at least 30 min to remove residual oxygen[1]. During the potentiostatic testing, a flow of NO (99.99%) with a rate of 20 mL min⁻¹ was continuously fed to the cathodic compartment. After electrolysis at specified potentials for 1 h, the aqueous and gas product are detected by the colorimetric methods and gas chromatography (GC), respectively.

Determination of NH₃

The generated NH₃ was determined by the indophenol blue method[2]. Typically, 0.5 mL of electrolyte was removed from the electrochemical reaction vessel and

diluted 10 times with deionized water. Then 2 mL of diluted solution was removed into a clean vessel followed by sequentially adding NaOH solution (2 mL, 1 M) containing C₇H₆O₃ (5 wt.%) and C₆H₅Na₃O₇ (5 wt.%), NaClO (1 mL, 0.05 M), and C₅FeN₆Na₂O (0.2 mL, 1wt.%) aqueous solution. After the incubation for 2 h at room temperature, the mixed solution was subjected to UV-vis measurement using the absorbance at 655 nm wavelength. The concentration-absorbance curves were calibrated by the standard NH₄Cl solution with a series of concentrations, and the NH₃ yield rate and Faradaic efficiency (FE) were calculated by the following equation[3]:

$$\text{NH}_3 \text{ yield} = (c \times V) / (17 \times t \times A) \quad (1)$$

Faradaic efficiency was calculated by the following equation:

$$\text{FE} = (5 \times F \times c \times V) / (17 \times Q) \times 100\% \quad (2)$$

where c ($\mu\text{g mL}^{-1}$) is the measured NH₃ concentration, V (mL) is the volume of electrolyte in the cathode chamber, t (s) is the electrolysis time and A is the surface area of CC ($1 \times 1 \text{ cm}^2$), F (96500 C mol^{-1}) is the Faraday constant, Q (C) is the total quantity of applied electricity.

Determination of N₂H₄

N₂H₄ in electrolyte was quantitatively determined by a Watt and Chrisp method [4]. Coloring solution was prepared by mixing 300 mL C₂H₅OH, 5.99 g C₉H₁₁NO and 30 mL HCl. Then, 5 mL color solution was added into 5 mL electrolyte. After the incubation for 20 min at room temperature, the mixed solution was subjected to UV-vis measurement using the absorbance at 455 nm wavelength. The concentration-absorbance curves were calibrated by the standard N₂H₄ solution with a series of concentrations.

Determination of NO₃⁻

NO₃⁻ in electrolyte was quantitatively determined by a reported method[5]. The electrolyte was collected and diluted to the detection range. 2 mL diluted electrolyte was mixed with 40 μL 1 M HCl containing 4.0 μL 0.8 wt% sulfamic acid. After the incubation for 20 min at room temperature, the mixed solution was subjected to UV-vis measurement using the absorbance at 220 nm wavelength. The concentration-absorbance curves were calibrated by the standard KNO₃ solution with a series of

concentrations.

Nuclear magnetic resonance measurement

¹H nuclear magnetic resonance (NMR) measurement was carried out using ¹⁵NO as the feed gas. After NORR electrolysis, 4 mL of electrolyte was removed from the electrochemical reaction vessel, which was concentrated to 1 mL and further acidized to pH 2. The obtained electrolyte was mixed with 0.1 mL of deuterium oxide (D₂O) containing 100 ppm of dimethyl sulphoxide (DMSO) and 70 μL of D₂O for NMR spectroscopy measurement (500 MHz Bruker superconducting-magnet NMR spectrometer).

Characterizations

X-ray diffraction (XRD) was conducted on a Rigaku D/max 2400 diffractometer. Transmission electron microscopy (TEM) and high-resolution transmission electron microscopy (HRTEM) were recorded on a Tecnai G² F20 microscope. X-ray photoelectron spectroscopy (XPS) analysis was collected on a PHI 5702 spectrometer. Electron paramagnetic resonance (EPR) measurements were conducted on a Bruker ESP-300 spectrometer. UV-vis absorption spectra were measured on MAPADA ULM 1912006 UV-vis spectrophotometer.

Calculation details

Spin-polarized DFT calculations were carried out using a Cambridge sequential total energy package (CASTEP). The Perdew–Burke–Ernzerhof (PBE) generalized gradient approximation (GGA) functional was used to model the exchange-correlation interactions. The DFT-D correction method with a Grimme scheme was used to describe the van der Waals interactions throughout the calculations. The electron wave functions were expanded using plane waves with a cutoff energy of 500 eV. The convergence tolerance was set to be 1.0×10^{-5} eV for energy and 0.02 eV Å⁻¹ for force. The Brillouin zone was sampled by 4×4×1 Monkhorst–Pack k-point mesh. SnS₂ (001) was modeled by a 2×2 supercell consisting of 16 Sn atoms and 32 S atoms. One central S atom was removed to construct the S vacancy with the S-vacancy density of 3.1 at%. A vacuum region of 15 Å was used to separate adjacent slabs. The adsorption energy (ΔE) is calculated as

$$\Delta E = E_{\text{ads/slab}} - E_{\text{ads}} - E_{\text{slab}} \quad (3)$$

where $E_{\text{ads/slab}}$, E_{ads} and E_{slab} are the total energies for adsorbed species on slab, adsorbed species and isolated slab, respectively.

The computational hydrogen electrode (CHE) model was adopted to calculate the Gibbs free energy change (ΔG) for each elementary step as follows:

$$\Delta G = \Delta E + \Delta ZPE - T\Delta S \quad (4)$$

where ΔE is the adsorption energy, ΔZPE is the zero-point energy difference and $T\Delta S$ is the entropy difference between the gas phase and adsorbed state. The entropies of free gases were acquired from the NIST database.

Molecular dynamics (MD) simulations were carried out using a force field type of Universal. The electrolyte system was geometrically optimized by setting the convergence tolerance of 2.0×10^{-5} kcal/mol for energy and 0.001 kcal/mol/Å for force. The non-bond interaction was processed by Ewald with accuracy of 10^{-5} Kcal/mol and the repulsive cutoff was chosen as 12 Å. The electrolyte system was set up by randomly placing 1000 H₂O, 50 NO molecules in the simulation box. After geometry optimization, the MD simulations were performed under the universal field with the total simulation time of 5 ns at a time step of 1 fs.

The radial distribution function (RDF) is calculated as

$$g(r) = \frac{dN}{4\pi\rho r^2 dr} \quad (5)$$

where dN is the amount of NO in the shell between the central particle r and $r+dr$, ρ is the number density of NO.

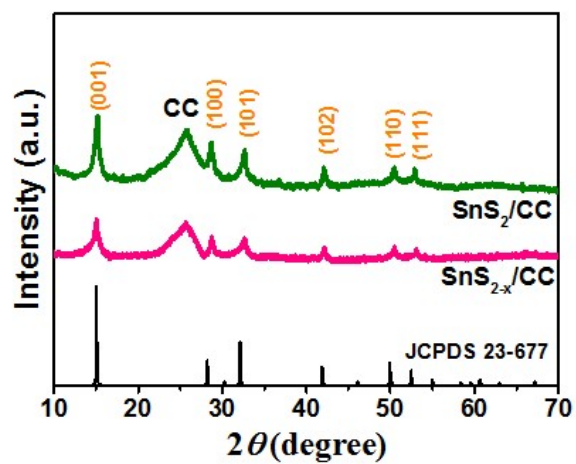


Fig. S1. XRD patterns of SnS₂/CC and SnS_{2-x}/CC.

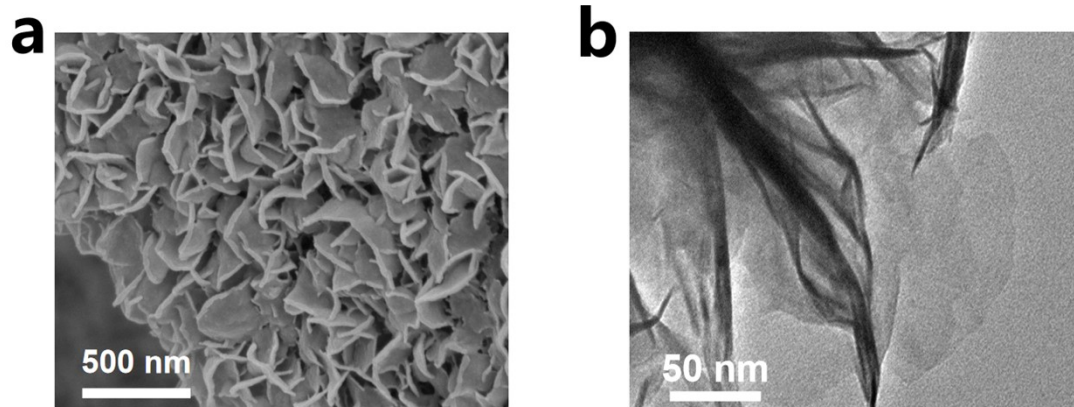


Fig. S2. (a) SEM and (b) TEM images of SnS₂ nanosheets.

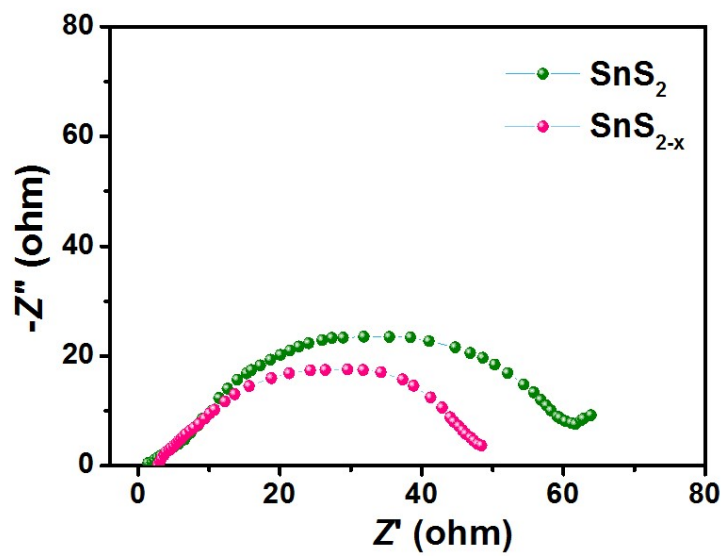


Fig. S3. Electrochemical impedance spectra of SnS_2/CC and $\text{SnS}_{2-x}/\text{CC}$.

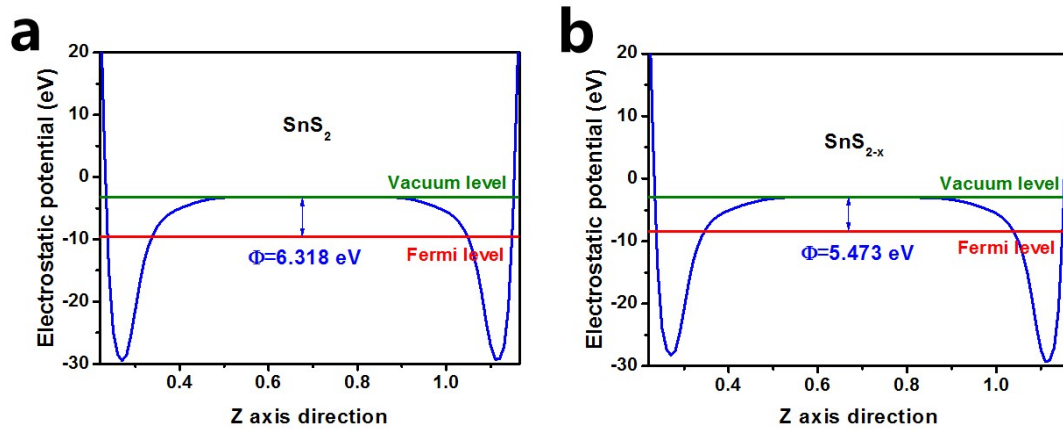


Fig. S4. Average potential profiles along c-axis direction for calculating the work functions of (a) SnS_2 and (b) SnS_{2-x} .

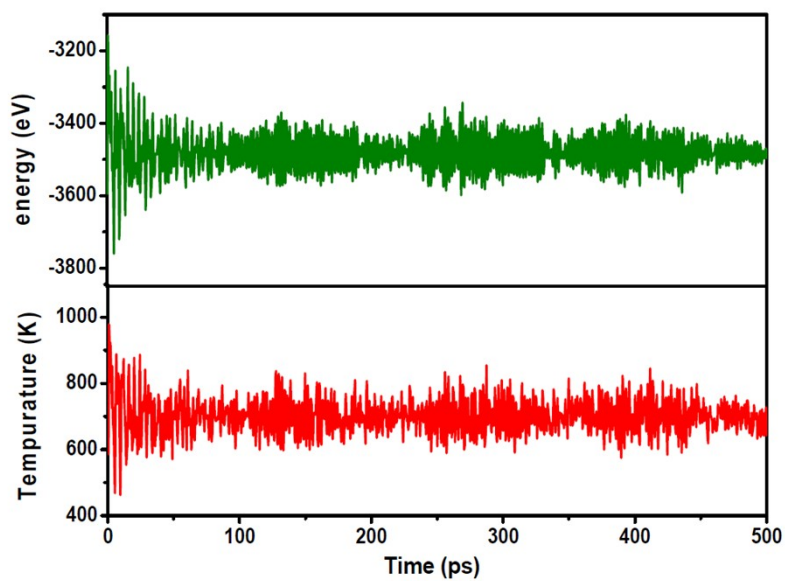


Fig. S5. Variations of energy and temperature during the AIMD simulation for assessing the thermodynamic stability of SnS_{2-x} .

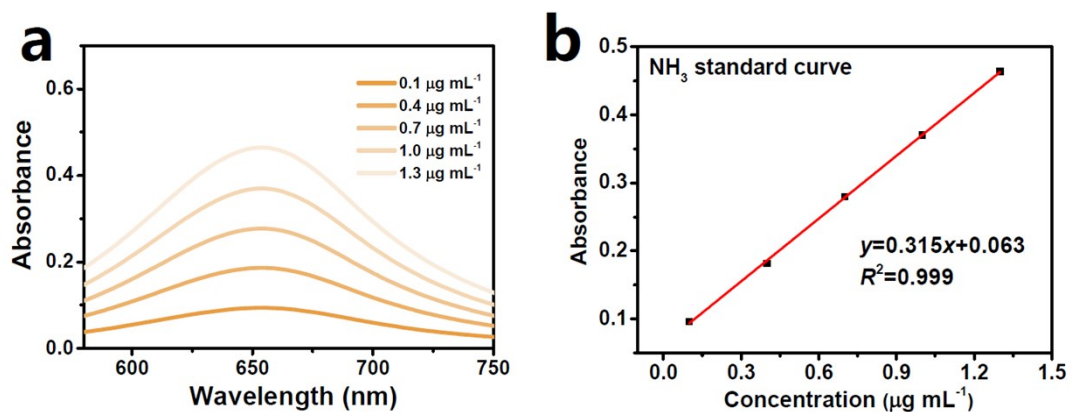


Fig. S6. (a) UV-vis absorption spectra of NH_4^+ assays after incubated for 2 h at ambient conditions. (b) Calibration curve used for the calculation of NH_3 concentrations.

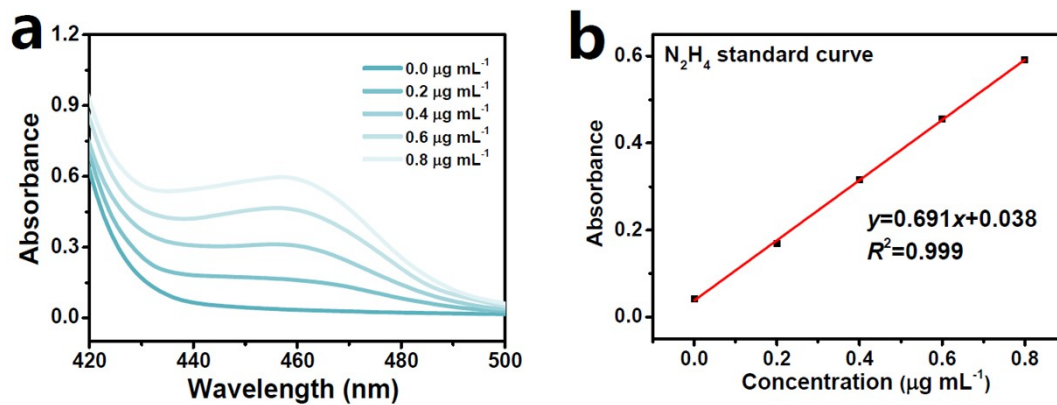


Fig. S7. (a) UV-vis absorption spectra of N_2H_4 assays after incubated for 20 min at ambient conditions. (b) Calibration curve used for calculation of N_2H_4 concentrations.

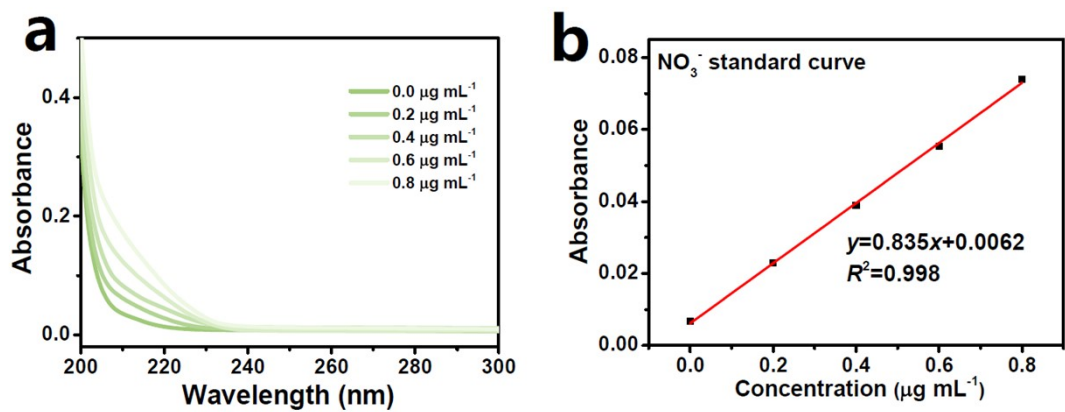


Fig. S8. (a) UV-vis absorption spectra of NO_3^- assays after incubated for 20 min at ambient conditions. (b) Calibration curve used for calculation of NO_3^- concentrations.

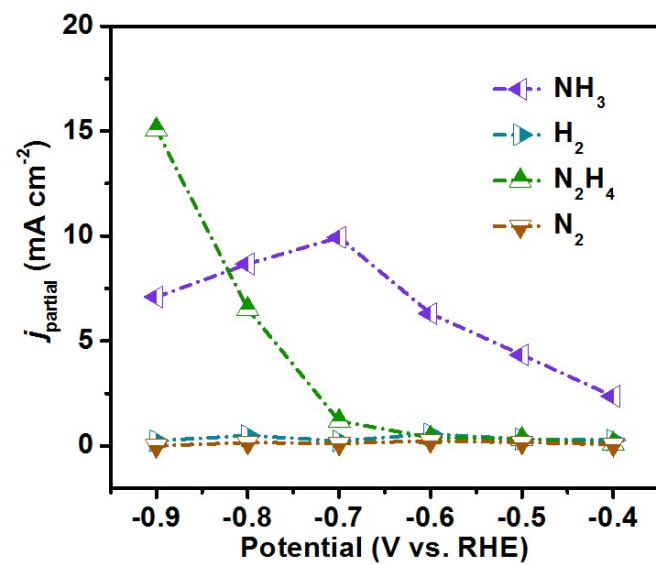


Fig. S9. Partial current densities of various products at different potentials.

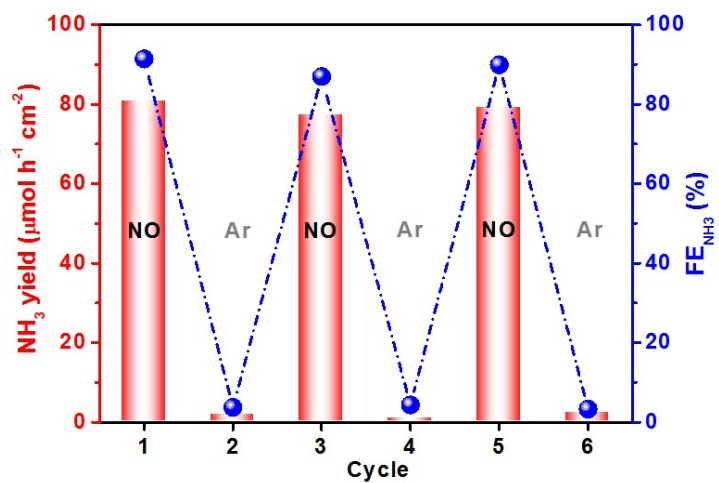


Fig. S10. NO–Ar gas switching experiment on SnS_{2-x}/CC at -0.7 V.

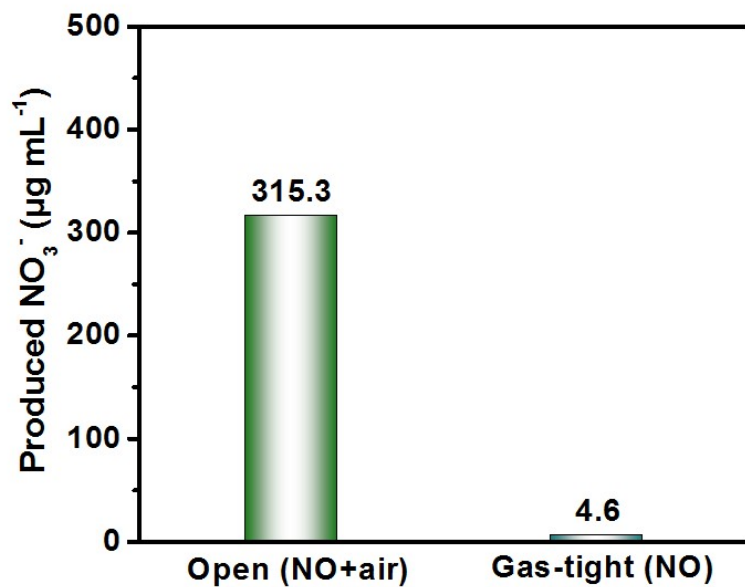


Fig. S11. Amounts of produced NO_3^- in open and gas-tight electrolytic cells.

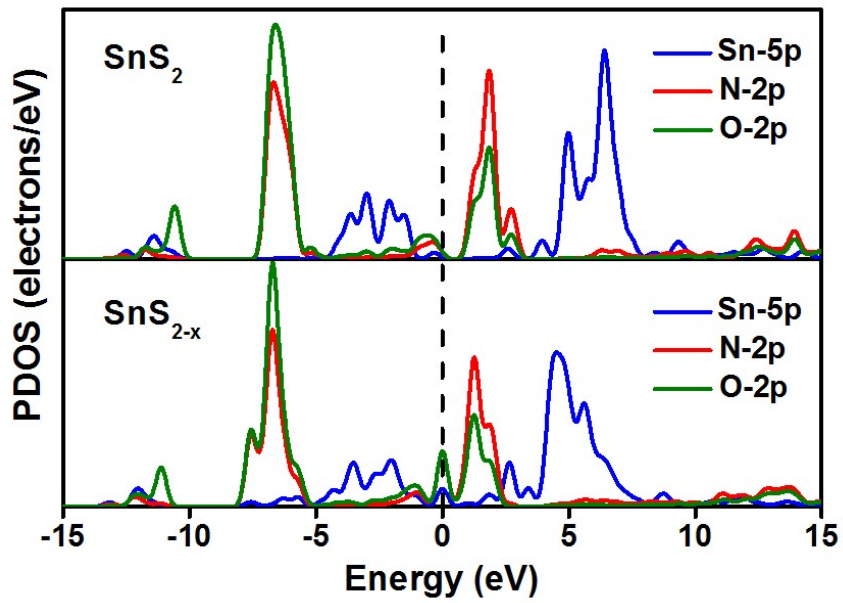


Fig. S12. PDOS profiles of absorbed NO on SnS₂ and SnS_{2-x}.

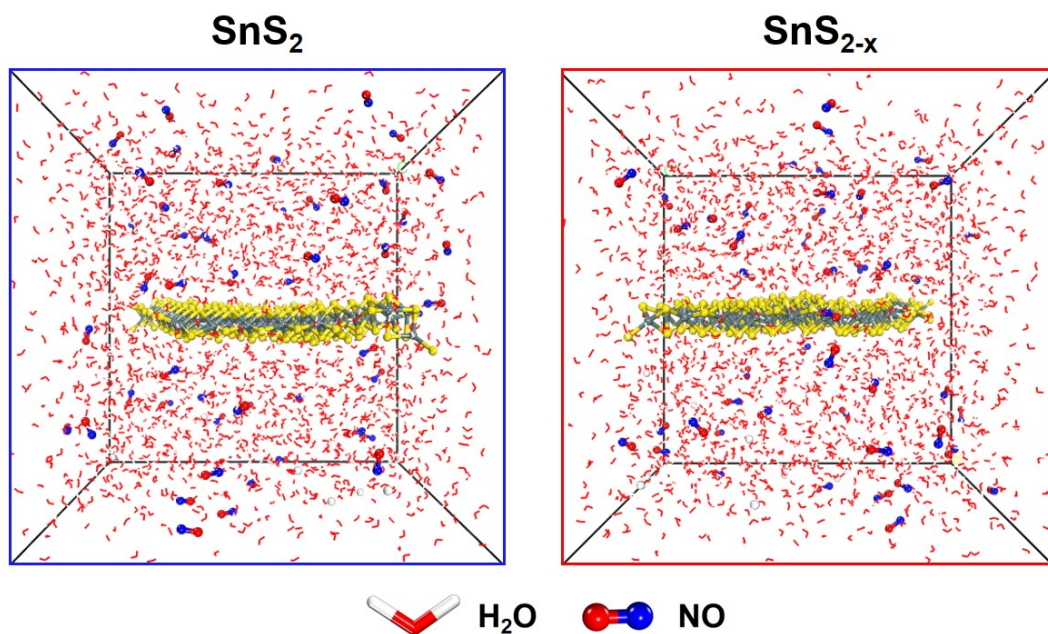


Fig. S13. Snapshots of the initial states for the dynamic process of NO adsorption on SnS₂ and SnS_{2-x} before MD simulations.

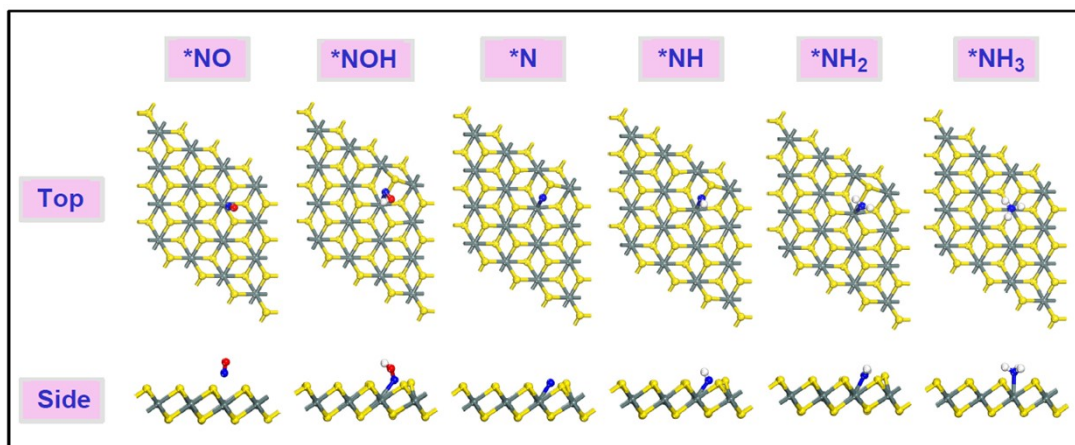


Fig. S14. The optimized atomic structures of the reaction intermediates on SnS₂.

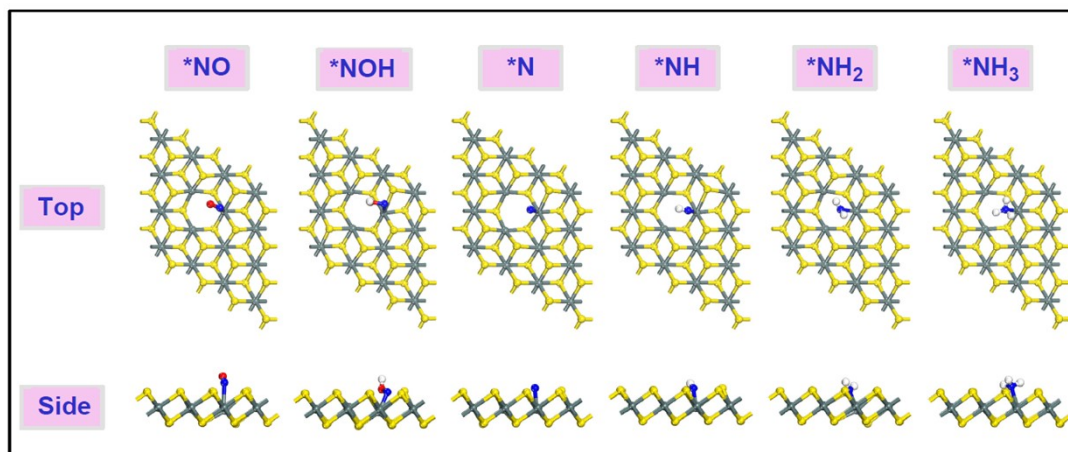


Fig. S15. The optimized atomic structures of the reaction intermediates on SnS_{2-x}.

Table S1. Comparison of the optimum NH₃ yield and FE_{NH3} for the recently reported state-of-the-art NORR electrocatalysts at ambient conditions.

Catalyst	Electrolyte	NH ₃ yield rate (μmol h ⁻¹ cm ⁻²)	FE _{NH3} (%)	Potential (V vs. RHE)	Ref.
Ni ₂ P/CP	0.1 M HCl	33.47	76.9	-0.2	[6]
Ru _{0.05} Cu _{0.95}	0.05 M Na ₂ SO ₄	17.68	64.9	-0.5	[7]
MoS ₂ /GF	0.1 M HCl	99.6	76.6	0.1	[8]
MnO _{2-x} NA/TM	0.2 M Na ₂ SO ₄	9.9	82.8	-0.7	[9]
Ni@NC	0.1 M HCl	34.6	72.3	0.16	[10]
Single atom Nb	0.1 M HCl	295.2	77.1	-0.6	[11]
a-B _{2.6} C@TiO ₂ /Ti	0.1 M Na ₂ SO ₄	216.4	87.6	-0.9	[12]
CoP/TM	0.2 M Na ₂ SO ₄	47.22	88.3	-0.2	[13]
CoS _{1-x} /CP	0.2 M Na ₂ SO ₄	44.67	53.62	-0.4	[14]
Bi NDs	0.1 M Na ₂ SO ₄	70.2	89.2	-0.5	[15]
SnS_{2-x}	0.5 M Na₂SO₄	78.6	90.3	-0.7	This Work

Table S2. ZPE and TΔS energies values of various species.

Species	ΔZPE (eV)	TΔS (eV)
*NO	0.18	0.13
*NOH	0.47	0.14
*N	0.08	0.03
*NH	0.36	0.05
*NH ₂	0.69	0.08
*NH ₃	1.04	0.13
*H	0.05	0.2

Supplementary references

- [1]. L. Zhang, J. Liang, Y. Wang, T. Mou, Y. Lin, L. Yue, T. Li, Q. Liu, Y. Luo, N. Li, B. Tang, Y. Liu, S. Gao, A. A. Alshehri, X. Guo, D. Ma and X. Sun, *Angew. Chem. Int. Edit.*, 2021, **60**, 25263-25268.
- [2]. P. Li, Z. Jin, Z. Fang and G. Yu, *Energy Environ. Sci.*, 2021, **14**, 3522-3531.
- [3]. Y. Wang, C. Wang, M. Li, Y. Yu and B. Zhang, *Chem. Soc. Rev.*, 2021, **50**, 6720-6733.
- [4]. G. W. Watt and J. D. Chrisp, *Anal. Chem.*, 1952, **24**, 2006-2008.
- [5]. L. C. Green, D. A. Wagner, J. Glogowski, P. L. Skipper, J. S. Wishnok and S. R. J. A. b. Tannenbaum, *Anal. Biochem.*, 1982, **126**, 131-138.
- [6]. T. Mou, J. Liang, Z. Ma, L. Zhang, Y. Lin, T. Li, Q. Liu, Y. Luo, Y. Liu, S. Gao, H. Zhao, A. M. Asiri, D. Ma and X. Sun, *J. Mater. Chem. A*, 2021, **9**, 24268-24275.
- [7]. J. Shi, C. Wang, R. Yang, F. Chen, N. Meng, Y. Yu and B. Zhang, *Sci. China Chem.*, 2021, **64**, 1493-1497.
- [8]. L. Zhang, J. Liang, Y. Wang, T. Mou, Y. Lin, L. Yue, T. Li, Q. Liu, Y. Luo, N. Li, B. Tang, Y. Liu, S. Gao, A. A. Alshehri, X. Guo, D. Ma and X. Sun, *Angew. Chem. Int. Ed.*, 2021, **133**, 25467-25472.
- [9]. Z. Li, Z. Ma, J. Liang, Y. Ren, T. Li, S. Xu, Q. Liu, N. Li, B. Tang, Y. Liu, S. Gao, A. A. Alshehri, D. Ma, Y. Luo, Q. Wu and X. Sun, *Mater. Today Phys.*, 2022, **22**, 100586.
- [10]. S. Sethuram Markandaraj, T. Muthusamy and S. Shanmugam, *Adv. Sci.*, 2022, **9**, 2201410.
- [11]. X. Peng, Y. Mi, H. Bao, Y. Liu, D. Qi, Y. Qiu, L. Zhuo, S. Zhao, J. Sun, X. Tang, J. Luo and X. Liu, *Nano Energy*, 2020, **78**, 105321.
- [12]. J. Liang, P. Liu, Q. Li, T. Li, L. Yue, Y. Luo, Q. Liu, N. Li, B. Tang, A. A. Alshehri, I. Shakir, P. O. Agboola, C. Sun and X. Sun, *Angew. Chem. Int. Ed.*, 2022, **61**, e202202087.
- [13]. J. Liang, W.-F. Hu, B. Song, T. Mou, L. Zhang, Y. Luo, Q. Liu, A. A. Alshehri, M. S. Hamdy, L.-M. Yang and X. Sun, *Inorg. Chem. Front.*, 2022, **9**, 1366-1372.
- [14]. L. Zhang, Q. Zhou, J. Liang, L. Yue, T. Li, Y. Luo, Q. Liu, N. Li, B. Tang, F. Gong, X. Guo and X. Sun, *Inorg. Chem. Front.*, 2022, **61**, 8096-8102.
- [15]. Y. Lin, J. Liang, H. Li, L. Zhang, T. Mou, T. Li, L. Yue, Y. Ji, Q. Liu, Y. Luo, N. Li, B. Tang, Q. Wu, M. S. Hamdy, D. Ma and X. Sun, *Mater. Today Phys.*, 2022, **22**.